Electronic and mechanical coupling between guest and host in carbon peapods

R. Pfeiffer,[1] H. Kuzmany,[1] T. Pichler,[1,2] H. Kataura,[3] Y. Achiba,[3] M. Melle-Franco,[4] and F. Zerbetto[4]

[1]*Universität Wien, Institut für Materialphysik, Strudlhofgasse 4, A-1090 Wien, Austria*
[2]*Institut für Festkörper und Werkstofforschung, D-01069 Dresden, Germany*
[3]*Tokyo Metropolitan University 1-1 Minami-Ohsawa, Hachioji, Tokyo 192-0397, Japan*
[4]*Dipartimento di Chimica "G. Ciamician," Universitá di Bologna, V. F. Selmi 2, 40126, Bologna, Italy*

Pristine single-wall carbon nanotubes (SWCNT's) filled with C_{60} are investigated with resonance Raman spectroscopy. Both totally symmetric modes of C_{60} exhibit a surprising splitting into two components with a slightly different resonance behavior and an apparent loss of polarization. The latter can be understood from a symmetry reduction of the fullerene molecules in the center of the tubes and/or by an anisotropy of the electric field seen by the C_{60} peas inside the SWCNT pods due to depolarization effects. The splitting is explained from molecular-dynamics simulations which show that the two bands emerge from a coupling of the C_{60} totally symmetric modes to the fullerene translational mobility inside the tube. The doublet is thus the spectroscopic fingerprint of different mobilities of C_{60} fullerenes in the tubes.

I. INTRODUCTION

New forms of carbon such as fullerenes and single-wall carbon nanotubes (SWCNT's) have been attracting considerable interest for a number of years.[1] A few years ago, these two new phases of carbon were combined when fullerenes were encapsulated inside SWCNT's (Ref. 2) and were produced in high yields by simultaneously heating opened SWCNT's and C_{60} in a sealed quartz tube.[3] These so-called "peapods" not only represent another family of nanostructured carbon, but are also prototypical materials grown in a concave nanospace. It can be expected that, e.g., highly unstable compounds can be stabilized inside SWCNT's. Examples have already been demonstrated in the form of fullerene polymers that were grown inside the tubes upon doping.[4] In related work, the nanotubes were also filled with other fullerenes,[5] or with inorganic materials.[6] These findings support the general idea that SWCNT's are ready to accept various types of molecules and further confirm the notion of being an ideal nanocavity for the creation of new materials.

The standard technique to analyze peapods is high-resolution transmission electron microscopy that yields good evidence for the filling. The quantitative determination of the concentration of C_{60} molecules in the tubes and the unraveling of the electronic properties, however, is difficult with this approach. Raman scattering has been proven to be another key experimental technique for the analysis of both fullerenes and SWCNT's. Its successful application to peapods is therefore not surprising. The resonance enhancement of the cross section for the fullerenes[7] allows to detect amounts of C_{60} smaller than 1% if encapsulated inside SWCNT's.[8] Two of the Raman allowed modes of the free C_{60} molecule belong to the nondegenerate A_g species, while eight modes are fivefold degenerate and of H_g symmetry. As a rule, the two A_g modes cannot split even if electric or mechanical fields of the guest tubes break the symmetry. Most prominent is the pentagonal pinch mode $A_g(2)$ located at 1469 cm^{-1} at room temperature. This mode has been used repeatedly as an analytical probe for the structural and elec-

tronic properties of C_{60}. A shift of its frequency can be expected in peapods since results from electron diffraction yield a slightly lower intercage distance for the encapsulated molecules than in C_{60} crystals. Importantly, the shorter distance cannot be taken as an indication of polymerization in the conventional sense, since the typical polymer lines are not observed in the peapod spectra and the C_{60}-C_{60} distances are still too large.

SWCNT's also have a number of significant Raman lines. For instance, the graphitic bands that derive from the G line are observed between 1500 and 1600 cm^{-1}. Around 200 cm^{-1} the radial breathing mode (RBM) of the tubes responds strongly to the Raman excitation. This mode is highly diagnostic for nanotubes since it scales as C/d where C is a constant and d is the diameter of the tubes.

In the work presented here, we focus on the behavior of the totally symmetric Raman lines of C_{60} in SWCNT's. Due to their simple nature they are most appropriate for extracting structural and dynamical information. A polarization analysis of the Raman response revealed a complete loss of the expected high polarization of these modes. This apparent loss of polarization can be due to a reduction of symmetry in the center of the tube and due to a reduction of the light field perpendicular to the axis inside the tube. The reduction of symmetry is ascribed to the hybridization of fullerene orbitals with tube orbitals and the subsequent capture of the highly anisotropic axial symmetry at the center of the nanotubes by the fullerene. On the other hand, the field seen by the peas enclosed in the tubes can be different from the outer field due to the high anisotropy of the tube polarizabilities.[9] Both effects—the reduction of molecular symmetry and the reduction of field symmetry—are shown to be relevant for the explanation of the experimental results. Another unexpected result was the splitting of the totally symmetric A_g modes which is quantitatively explained by a dynamical interaction between the C_{60} molecules and the tube cages. Eventually, it turns out to originate from a coupling between translational and vibrational motion in the systems.

69 035404-1

TABLE I. Mode frequencies and observed depolarization ratios for diamond, SWCNT's, C_{60}, and peapods. Frequencies for lines with several components are first moments. Excitation was at 90 K for 488 nm. Double prime lines are listed as excited with 647 nm. All intensities used were integrated areas.

Crystal	Mode	Frequency (cm^{-1})	Depolarization
Diamond	F_{2g}	1333	0.74
SWCNT's	RBM	170	0.3
	G lines	1575	0.3
C_{60}, polycrystalline	$H_g(2)$	430	0.3
	$A_g(1)$	497	0.055
	$H_g(7)$	1426	0.44
	$A_g(2)$	1469	0.13
Peapods	$H_g(2)$	430	0.41
	$A_g(1)'$, $A_g(1)''$	490,502	0.39,0.35
	$H_g(7)$	1426	0.3
	$A_g(2)'$, $A_g(2)''$	1466,1475	0.33,0.3

II. EXPERIMENT

The nanotubes were prepared by laser desorption and were purified and filled as described previously.[3] After filling with C_{60} the resulting mats of bundled tubes (peapods) were vacuum annealed at 800 K to get rid of any nonencapsulated C_{60} molecules. Measurements of the filling ratio using bulk sensitive electron-energy-loss spectroscopy[10] and Raman spectroscopy[8] revealed a maximum C_{60} occupancy of about 70%. Three sets of samples were investigated and are labeled A, B, and C in the following. Sample A had the largest diameters with a mean value of 1.40 nm and the highest degree of filling. The mean diameters for the other samples were 1.34 nm and 1.31 nm for B and C, respectively, as evaluated from the first and second spectral moments of the RBM.

Raman spectra were recorded for laser lines extending from 1.8 to 2.6 eV at 90 and 20 K using a Dilor *xy* triple spectrometer calibrated for intensities in 180° backscattering geometry. For 2.4- and 2.5-eV excitation energy temperature-dependent Raman spectra were also recorded between 20 and 600 K.

Additionally, we performed polarized Raman studies at 90 K. This means, for every sample two spectra, I_{HV} and I_{VV}, were recorded. In *HV* experiments the polarization of the incident light is perpendicular to the polarization of the analyzer sheet in front of the detector while in *VV* experiments both polarizations are parallel. In our setup we kept the polarization of the analyzer constant and used a $\lambda/2$ platelet to turn the polarization of the incident light by 90°. The two types of recorded spectra allowed to evaluate the depolarization ratio $\rho = I_{HV}/I_{VV}$. The polarization experiments were tested for the F_{2g} mode of polycrystalline diamond and for the totally symmetric modes of single crystal C_{60}. The values of ρ obtained for the two materials were 0.74 and 0.01, respectively, in excellent agreement with expected values of 3/4 and 0 (see Table I).

III. EXPERIMENTAL RESULTS

A. Unpolarized Raman spectra

For strongly filled peapods, all fundamental Raman lines of the encaged C_{60} peas, with the known exception of
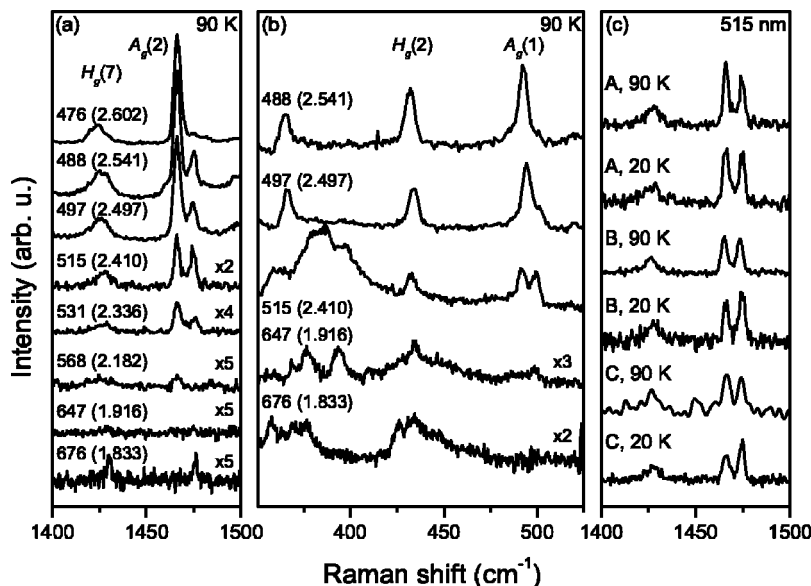
FIG. 1. Tangential part (a) and radial part (b) of the Raman spectrum at 90 K for peapod material A excited with different lasers as indicated in nm (eV). The strong line around 425 cm^{-1} is the $H_g(2)$ mode of the C_{60} peas. (c) Raman response of the tangential C_{60} modes for tubes with three different diameters at 20 and 90 K for 515 nm excitation.

$H_g(8)$, were detected with blue laser excitation. A detailed analysis of the spectra for the different samples and for different laser excitations revealed surprising results, as shown for the tangential and for the radial modes in Fig. 1.

At 1466 cm^{-1}, slightly below (≈ 3 cm^{-1}) its position in C$_{60}$ single crystals and films, we observe the pentagonal pinch mode with a decreasing cross section for increasing laser wavelength. At 1475 cm^{-1}, a second line appears in the $A_g(2)$ region that increases in relative intensity for shifting the excitations from the blue to the red. For green laser excitation both lines are of equal intensity and eventually the higher-frequency component dominates. For simplicity the two lines will be assigned as $A_g(2)'$ and $A_g(2)''$, respectively. Significantly, the same behavior is observed for the other totally symmetric $A_g(1)$ mode of C$_{60}$ as demonstrated in Fig. 1(b). For excitation with the blue lasers, we see only the component $A_g(1)'$, at 490 cm^{-1}. For green laser excitation, the line splits into $A_g(1)'$ and $A_g(1)''$, with the latter located at 502 cm^{-1}. Eventually, for red laser excitation, only the line $A_g(1)''$ is observed. The additional features around 375 and 425 cm^{-1} are overtones of the RBM of the tubes resonating with the E_{22}^s and E_{33}^s transition in the semiconducting tubes.

A detailed analysis of the resonance response was performed for the two components of the $A_g(2)$ mode. The maximum resonance is reached for different laser energies, 2.54 eV for the $A_g(2)'$ and 2.41 eV for the $A_g(2)''$ line.[11] In addition, the latter exhibits a second resonance, which reaches its maximum in the red spectral region at 1.80 eV. Similar laser selective results were obtained for the degenerate H_g modes. Since these modes always split for C$_{60}$ molecules in a crystal field such results are not as informative as those of the A_g modes and will therefore not be discussed in the following.

Figure 1(c) demonstrates the splitting for different tube materials at 90 and 20 K. Thinner tubes tend to yield a stronger $A_g(2)''$ component. Additionally, the intensity of the $A_g(2)''$ component seems to increase relative to the $A_g(2)'$ when the samples were cooled down from 90 to 20 K.

B. Temperature dependence

In order to elaborate on the latter result, we recorded temperature-dependent Raman spectra of sample A. The top part of Fig. 2 shows the 515-nm spectra of this sample for different temperatures from 80 to 590 K after renormalization to the G modes and subtraction of the G-mode backgrounds. While the height of the $A_g(2)'$ component does not change much the intensity of the $A_g(2)''$ line decreases with increasing temperature. Additionally, both lines become broader and shift downwards with increasing temperature.

To demonstrate the different temperature behavior of the two components more clearly, their intensity ratios are plotted in Fig. 2 (bottom) vs temperature. To do this the spectra were fitted between 1440 and 1500 cm^{-1} with two Voigtian lines, keeping the Gaussian widths constant for both modes and all temperatures. As long as the $A_g(2)''$ mode was clearly observable, the distance between the Voigtians was varied during the fit. Later on, we kept the distance constant
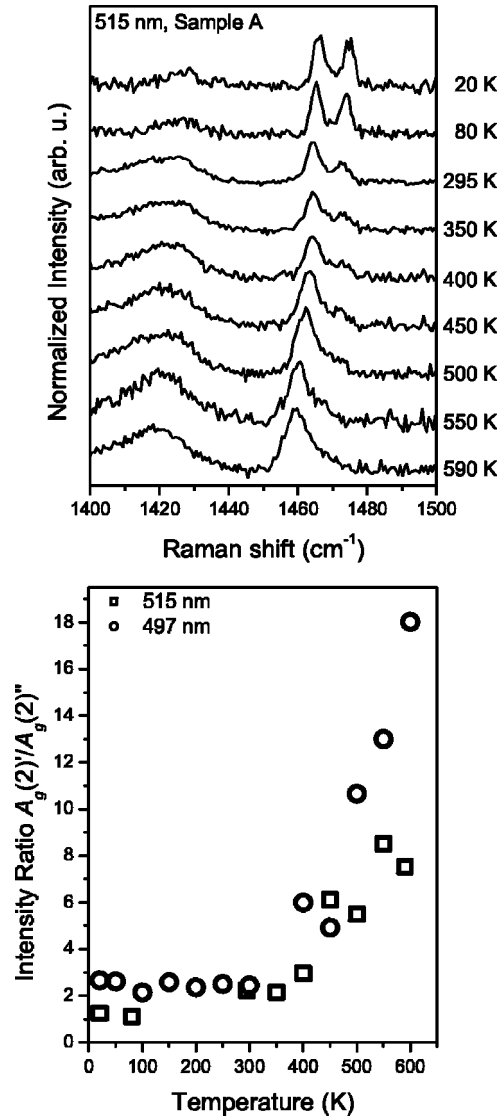
FIG. 2. Top: 515-nm Raman spectra of peapod sample A for several temperatures from 80 to 590 K. The spectra were scaled such that the height of the G mode was normalized to 1. Bottom: Intensity ratios of the $A_g(2)'$ to the $A_g(2)''$ component vs temperature for 515- and 497-nm excitations of sample A.

at the average value of 8.3(1) cm^{-1}, as found for the lower temperatures. However, even without this constraint a fit revealed that both modes shift in parallel.

Within experimental error, the intensity ratios remain constant below 300 K. For higher temperatures the intensity of the higher frequency component $A_g(2)''$ decreases rapidly and hence the intensity ratio increases.

C. Polarized Raman spectra

The splitting of the totally symmetric C$_{60}$ modes in the tubes is rather surprising. One possibility for this could be a dimerization of the peas along the tube (Davydov splitting). If that was the case, the symmetry of the two components $A_g(2)'$ and $A_g(2)''$ would be different. One would remain totally symmetric, while the other would be nontotally sym-

metric. Polarized Raman experiments are commonly used to reveal the symmetry of a particular mode.

In single crystals the depolarization ratio ρ as defined above is determined by the Raman tensor components selected by the scattering geometry. In polycrystalline material, such as our buckypaper, angular averaged values of the Raman tensor components are needed. After this averaging process two tensor derived quantities, namely, the trace $3a$ and the anisotropy τ remain as the transformation invariant quantities. With these, the depolarization ratios can be written as[12]

$$\rho = \frac{I_{\mathrm{HV}}}{I_{\mathrm{VV}}} = \frac{3\tau^2}{45a^2 + 4\tau^2}. \tag{1}$$

If the symmetry is higher than C_3, the Raman tensor for a totally symmetric mode has nonzero elements only in the main diagonal. That is, the scattered light has the same polarization as the incident light. If the analyzer has the same polarization (VV) the mode is visible and if the polarization of the analyzer is perpendicular to the incident light (HV) the mode should not be observable. Totally symmetric modes have therefore a depolarization ratio of $\rho = 0$. If the symmetry of the scatterer is lower than C_3, however, off-diagonal elements exist and ρ becomes $\neq 0$ even for totally symmetric modes.

According to the above description, a polarization analysis of the two components should give, in principle, indications about the presence of Davydov splitting. Interestingly, for the $A_g(2)'$ and $A_g(2)''$ modes of the C_{60} peas the observed depolarization ratio turned out to be the same for the two components [see Fig. 3 (bottom)]. Even more surprising was the value of 0.3 for the ratio itself. This is in strong contrast to a control experiment on a polycrystalline film of C_{60}, which yielded a very low depolarization ratio for the totally symmetric modes and a reasonable depolarization ratio for the H_g derived modes, as depicted in Table I and Fig. 3 (top).

The depolarization ratios for the mainly totally symmetric nanotube modes, namely the RBM and the graphitic mode, were also surprisingly large but in agreement with previous measurements.[13] In this case large values for ρ can be understood, even without considering the asymmetry of the field, since the strong electronic anisotropy of the tubes results in a dominance of the zz component of the Raman tensor, where the z direction is along the tube axis. As a consequence, both the anisotropy τ and the trace a are dominated by the zz component as well and the depolarization ratio for the totally symmetric modes becomes 0.35, in very good agreement with experiments.

Depolarization ratios are often difficult to measure or involve errors from alignment for the recording of the two required spectra. In order to confirm the intrinsic nature of the observed depolarization ratio we evaluated a ratio of depolarization ratios, hereafter called depolarization factor ratio (DPFR). This quantity is defined as

$$\mathrm{DPFR} = \frac{I_{\mathrm{VV}}(A_g(i))/I_{\mathrm{VV}}(H_g(j))}{I_{\mathrm{HV}}(A_g(i))/I_{\mathrm{HV}}(H_g(j))} = \frac{\rho(H_g(j))}{\rho(A_g(i))}, \tag{2}$$
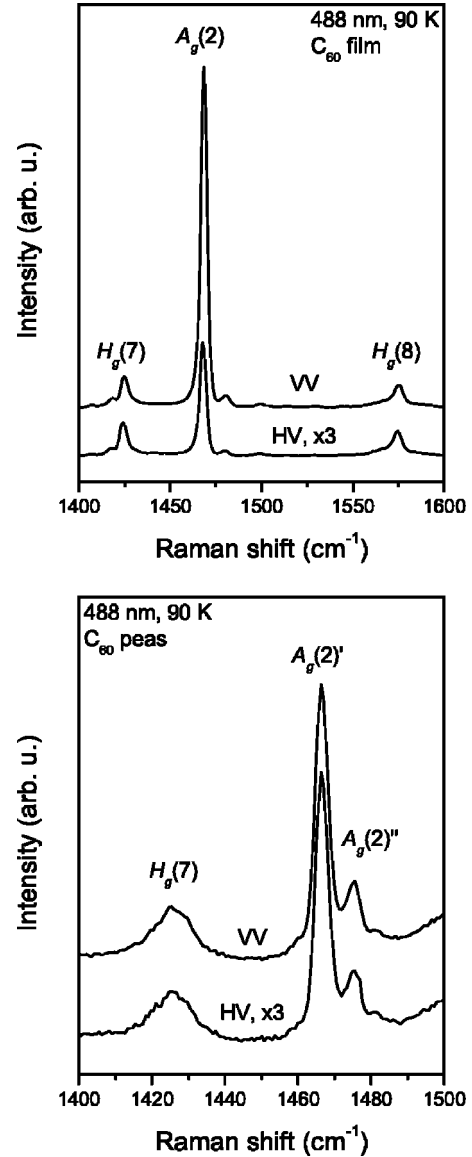
FIG. 3. Polarized Raman spectra of a C_{60} film (top) and C_{60} peapod sample A (bottom) recorded with 488 nm at 90 K. VV means parallel polarizations between incident light and analyzer and HV means that the polarization of the incident light is perpendicular to analyzer.

where i and j are any allowed Raman active modes of C_{60}. Only relative intensities from one spectrum appear in the equation. The DPFR is therefore highly independent from the experimental conditions. Since the DPFR is the ratio of the depolarization of a nontotally symmetric to a totally symmetric mode it should be much larger than 1. This is indeed the case for C_{60} in the film, but not for the molecules in the tubes. Figure 4 compares the DPFR for peapods and polycrystalline C_{60}. The large values for the C_{60} film are as expected and demonstrate that the depolarization is stronger for the A_g modes than for the H_g modes. The values around one obtained for the C_{60} peas are unusual, but confirm the results from the direct depolarization ratio, measurements. As a practical consequence of the similarity in depolarization ra-
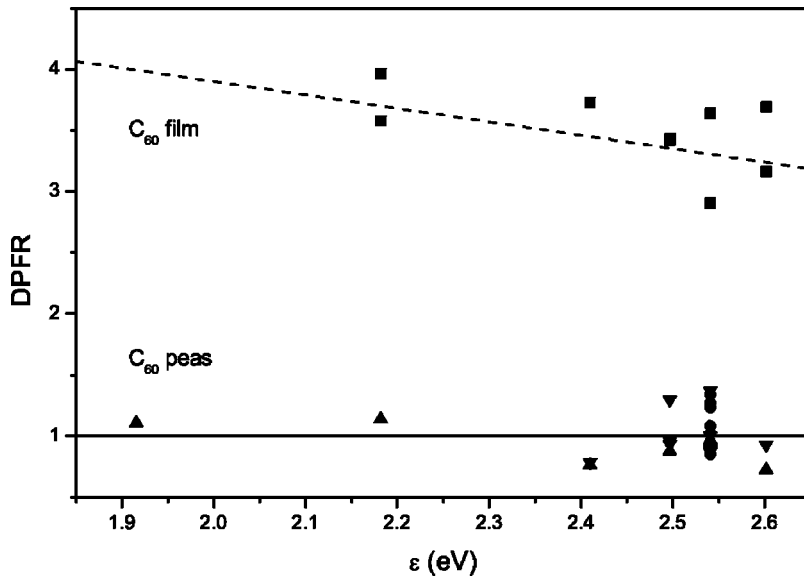
FIG. 4. Depolarization factor ratio DPFR as defined from Eq. (2) vs laser energy for a C_{60} film [■ for $A_g(2)$ vs $H_g(7)$ and $H_g(8)$] and for molecules in the tubes [▼ for $A_g(2)'/H_g(7)$, ▲ for $A_g(2)''/H_g(7)$, and ● for $A_g(1)$ vs various $H_g(j)$ in the radial region].

tios, all A_g derived and H_g derived peapod modes can no longer be discriminated on this basis (see Table I).

IV. MOLECULAR-DYNAMICS SIMULATIONS

In order to obtain possible interpretations of the splitting we performed computer simulations on peapod systems in addition to the experiments. A phenomenological approach using vibronic mixing[14] could not pinpoint the origin of the splitting. In a harmonic approximation, only shifts of the $A_g(2)$ frequency were observed with values depending on the tube diameter. The result implies that for any monomodal diameter distribution, no splitting can be expected from this approach.

We therefore went beyond the harmonic approximation using molecular-dynamics calculations. The van der Waals interactions between pairs of nonchemically bonded atoms were described by the relevant part of the MM3 potential.[15] MM3 was successful in the description of the subtle effects that lead to C_{60} spinning in clusters.[16] The present approach was recently used to model the effect of permanent twisting of SWCNT's[17] and a variety of other properties of all carbon peapods.[18]

The cutoff for the interatomic potential was set to 10 Å, after checking that the procedure gave accurate results for graphite. Periodic boundary conditions were used axially. When partial filling ratios with more than one C_{60} per tube were simulated, the free region inside the nanotube was set to at least 10 Å on each side of the encapsulated molecule(s). The Fourier transform of the velocity autocorrelation function gives vibrational frequencies that include both anharmonicities and coupling of different degrees of freedom and is able to pick up a number of subtle effects in complicated materials.[19,20]

The peapods were first equilibrated at $T = 298$ K in the NVT ensemble (constant number of particle, volume, and temperature). Then the vibrational spectrum was calculated with a dynamics at constant energy. Typically, equilibration was reached after 30 ps. Convergence of the potential energy

to a plateau ensured that it had really occurred. The NVE (constant number of particle, volume, and energy) dynamics was performed for at least 70 ps with time steps of 1 fs. The spectral resolution of the simulation was at least 1 cm^{-1}. Initially, the simulations were run for free C_{60} and for a single $C_{60}@(10,10)$. Both systems gave a single peak for the $A_g(2)$ mode with a difference of less than 1 cm^{-1}. The shift is even smaller than the values calculated in the harmonic approximation for the two cases.

Subsequently and more realistically, with respect to the nature of the experimental conditions, two types of molecular-dynamics simulations were performed on a system with three C_{60} peas inside a supercell of (10,10) made by 12 unit cells of the tube. In the first simulation, the triplet of molecules was allowed to diffuse freely in the tube, in the second, the diffusional dynamics was frozen. Upon Fourier transform of the two dynamics, two distinct peaks were found: the first was slightly more than 2 cm^{-1} above that of free C_{60} (and corresponded to the "frozen" diffusion), while the second was more than 4 cm^{-1} below that of free C_{60}. The calculated separation of 6 cm^{-1} is slightly less than the values observed experimentally but of the right order. It arises from the same peapod and can be assumed to be a general feature of peapods. The convolution of all the splittings for all CNT's present in the sample maintains the observed splitting of the $A_g(2)$ mode. Importantly, while the simulations show that the splitting arises from the coupling of the $A_g(2)$ mode with the translational motion of C_{60} inside the tube, one should remember that lack of C_{60} mobility could be due to a variety of reasons that range from full packing to the presence of physical obstructions in the tube.

V. DISCUSSION

The disappearance of the polarization for the bands of the totally symmetric lines of $C_{60}@SWCNT$'s and their splitting into doublets is unexpected. The loss of the Raman polarization can be due to a complete geometrical symmetry loss as a consequence of orbital hybridization. The latter effect has

TABLE II. List of tubes and their site symmetry in the center for the diameter range of the experiment.

(9,6)	C_3	(10,4)	C_2	(7,7)	D_{7d}	(8,8)	D_{8h}	(11,8)	C_1
(12,3)	C_4	(12,6)	C_6	(10,10)	D_{10h}	(8,5)	C_1	(10,7)	C_1
(9,9)	D_{9d}	(13,1)	C_1	(9,8)	C_1	(7,6)	C_1	(11,9)	C_1
(10,3)	C_1	(12,5)	C_1	(13,5)	C_1	(13,6)	C_1	(11,2)	C_1
(10,8)	C_2	(10,9)	C_1						

been reported from tunneling experiments[21] and from theoretical considerations.[22] Most of the tubes in the diameter range under consideration have a site symmetry C_1 in their center as depicted in Table II. This means all vibrations from C_{60} in the tubes belong to the A irreducible representation and therefore similar values for τ and a are expected. Tubes with higher site symmetry exist, but only for armchair and a few metallic chiral tubes. Even for those tubes the anisotropy τ for the totally symmetric modes is not zero, which means the depolarization ratio will be finite.

Polarization experiments on SWCNT's and derived samples are complicated by the large aspect ratio of the tubes. For an unpolarized field outside the tubes the ratio between the field components parallel and perpendicular to the tube axis inside the tubes is proportional to $\exp[(\alpha_\parallel - \alpha_\perp)d]$, where $\alpha_\parallel$ and $\alpha_\perp$ are the absorption coefficients parallel and perpendicular to the tube axis as derived from a linear response function, respectively. Since the thickness of the wall d is only one atomic layer one might think that the field inside the tube is almost the same as the field outside the tube. However, Benedict *et al.*[9] reported that the aspect ratio of the tubes causes a strong anisotropy of the static polarizability of SWCNT's. That is, the electric field inside the tube is strongly reduced when the outer field is oriented perpendicular to the tube axis because of induced surface dipoles. In a good approximation this may also be valid for nonstatic fields. This means the induced surface dipoles provide an additional contribution to the response function.

Krupke *et al.*[23] have used this effect for the separation of semiconducting and metallic SWCNT's in a solution of individual tubes. Marinopoulos *et al.*[24] used a theoretical analysis based on density functional theory including local field effects and cross-correlation terms to study the depolarization effect in optical absorption spectra of thin SWCNT's. Their calculations confirm this effect for isolated tubes but found it strongly reduced for tubes in bundles as is the case in our measurements.

The observed depolarization ratios for the C_{60} peas could also be explained by the above described strong anisotropy of the tube polarizability.[9] Assuming full action of the depolarization effect this implies that the observed intensities depend on the angle φ between the direction of, e.g., the V polarized analyzer and the tube axis. From this one may expect an intensity $I_{VV} \propto (E\cos^2\varphi)^2$ and an intensity $I_{HV} \propto (E\cos\varphi\sin\varphi)^2$ for VV and HV experiments, respectively. Since the tubes in our sample were not aligned these intensities have to be averaged over all angles φ resulting in $I_{VV} \propto 3\pi/16$ and $I_{HV} \propto \pi/16$, which would give a depolarization ratio of $\rho = 1/3$. In nanotube bundles the action of the depolarization effect is considerably reduced as was demon-

strated by Marinopoulos *et al.*[24] It is therefore evident that the observed depolarization behavior does not originate exclusively from the depolarization effect.

As a consequence of the discussion presented above, the symmetry loss in the measurement of the depolarization ratio cannot be considered any more as a criterion for dimerization or Davidov splitting in either of the two cases. From inspecting many TEM pictures and from discussions with specialists,[25] however, dimerization of the fullerenes is not expected to occur according to the state-of-the-art knowledge. On the other hand, neither the symmetry loss itself nor the reduction of the total field can explain the line splitting for a nondegenerate totally symmetric mode. As it turns out, a considerable guest-host interaction including a collective dynamical response of the fullerenes is capable to explain the splitting.

From the results for the computational approaches it is clear that the splitting can be explained by anharmonic effects in the dynamics of the fullerene motion. The lack of a calculated splitting in the dynamics of a single C_{60} inside a (10,10) CNT underlines that the splitting is linked to the degree of mobility of C_{60} inside the tube. In fact, while C_{60} is highly mobile inside a pod and experiences the effect of very small energy barriers for its motion[26] a single fullerene is certainly more free to drift along the tube than a set of three. In other words it resembles more that of a really free C_{60} than the present case. In order to confirm the role of the mobility we introduced constraints in the dynamics so that the axial diffusion of fullerenes was inhibited. This was accomplished in a simple way by freezing one of every three molecules. This assumption allowed to sample only the part of the motion in the doublet that is not coupled with any form of translations. The dynamics with reduced mobility also provided two peaks. However, numerically the splitting was only 4 cm^{-1} and shifted compared to that obtained before with the first peak located at the frequency of the free C_{60}. Their average therefore corresponds to the higher-energy component of the doublet.

The constraints in the dynamics may or may not correspond to an actual physical situation, where some C_{60} molecules are actually locked in place. It is important to notice, however, that the splitting naturally emerges in simulations where no constraints are present and that the higher frequency component corresponds to a suppressed dynamics where the $A_g(2)$ mode is less coupled to the translational degree of freedom inside the CNT. This interpretation is fully consistent with the results from the temperature and tube diameter dependence of the $A_g(2)'/A_g(2)''$ intensity ratio. For higher temperatures and larger diameter tubes the num-

ber of blocked C_{60} molecules decreases which reduces the response from this species.

VI. SUMMARY

In summary, we have shown that the typical depolarization ratio of the totally symmetric modes of C_{60} is completely lost when these fullerenes are inside SWCNT's. This might be due to a complete loss of symmetry of the enclosed peas or because the outer fields are screened by the tubes depending on their polarization with respect to the tube axis. Additionally, we have shown that these totally symmetric bands are split for the encaged fullerenes. We attribute this to an additional mechanical coupling between the peas and the pods that results in a lowered mobility for some peas. Molecular-dynamics calculations show that such a splitting appears only for peapods where the C_{60}'s, embedded in a tube, undergo the additional interaction resulting from the motion of the peas. Both the tube-C_{60} and the C_{60}-C_{60} interactions are necessary to produce the splitting. Indeed, we performed similar calculations for C_{60} in the solid, which did not give the doublet but only a single line. The molecular-dynamics simulation shows that the low-frequency part of the doublet of the $A_g(2)$ mode is the spectroscopic fingerprint of a mobility of C_{60} larger than that associated with the other C_{60} molecules which respond at the higher frequency.

[1] M. S. Dresselhaus, G. Dresselhaus, and P. C. Eklund, *Science of Fullerenes and Carbon Nanotubes* (Academic Press, San Diego, 1996).

[2] B.W. Smith, M. Monthioux, and D.E. Luzzi, Nature (London) **396**, 323 (1998).

[3] H. Kataura, Y. Maniwa, T. Kodama, K. Kikuchi, K. Hirahara, K. Suenaga, S. Iijima, S. Suzuki, Y. Achiba, and W. Krätschmer, Synth. Met. **121**, 1195 (2001).

[4] T. Pichler, H. Kuzmany, H. Kataura, and Y. Achiba, Phys. Rev. Lett. **87**, 267401 (2001).

[5] K. Hirahara, K. Suenaga, S. Bandow, H. Kato, T. Okazaki, H. Shinohara, and S. Iijima, Phys. Rev. Lett. **85**, 5384 (2000).

[6] R.R. Meyer, J. Sloan, R.E. Dunin-Borkowski, A.I. Kirkland, M.C. Novotny, S.R. Bailey, J.L. Hutchison, and M.L.H. Green, Science **289**, 1324 (2000).

[7] M. Matus, H. Kuzmany, and W. Krätschmer, Solid State Commun. **80**, 839 (1991).

[8] H. Kuzmany *et al.*, Appl. Phys. A: Mater. Sci. Process. **76**, 449 (2003).

[9] L.X. Benedict, S.G. Louie, and M.L. Cohen, Phys. Rev. B **52**, 8541 (1995).

[10] X. Liu, T. Pichler, M. Knupfer, M.S. Golden, J. Fink, H. Kataura, Y. Achiba, K. Hirahara, and S. Iijima, Phys. Rev. B **65**, 045419 (2002).

[11] R. Pfeiffer, H. Kuzmany, W. Plank, T. Pichler, H. Kataura, and Y. Achiba, Diamond Relat. Mater. **11**, 957 (2002).

[12] H. Kuzmany, *Solid-State Spectroscopy: An Introduction* (Springer-Verlag, Berlin, 1998).

[13] K. Kneipp, A. Jorio, H. Kneipp, S.D.M. Brown, K. Shafer, J. Motz, R. Saito, G. Dresselhaus, and M.S. Dresselhaus, Phys. Rev. B **63**, 081401(R) (2001).

[14] W.-Y. Chiang and J. Laane, J. Chem. Phys. **100**, 8755 (1994).

[15] N.L. Allinger, Y.H. Yuh, and J.H. Lii, J. Am. Chem. Soc. **111**, 8551 (1989).

[16] M.S. Deleuze and F. Zerbetto, J. Am. Chem. Soc. **121**, 5281 (1999).

[17] M. Melle-Franco, M. Prato, and F. Zerbetto, J. Phys. Chem. A **106**, 4795 (2002).

[18] M. Melle-Franco, H. Kuzmany, and F. Zerbetto, J. Phys. Chem. B **107**, 6986 (2003).

[19] C.-A. Fustin, D.A. Leigh, P. Rudolf, D. Timpel, and F. Zerbetto, ChemPhysChem **1**, 97 (2000).

[20] D.A. Leigh, S.F. Parker, D. Timpel, and F. Zerbetto, J. Chem. Phys. **114**, 5006 (2001).

[21] D.J. Hornbaker, S.-J. Kahng, S. Misra, B.W. Smith, A.T. Johnson, E.J. Mele, D.E. Luzzi, and A. Yazdani, Science **295**, 828 (2002).

[22] S. Okada, S. Saito, and A. Oshiyama, Phys. Rev. Lett. **86**, 3835 (2001).

[23] R. Krupke, F. Hennrich, H.v. Löhneysen, and M.M. Kappes, Science **301**, 344 (2003).

[24] A.G. Marinopoulos, L. Reining, A. Rubio, and N. Vast, Phys. Rev. Lett. **91**, 046402 (2003).

[25] D. E. Luzzi and A. Yazdani (private communication).

[26] S. Berber, Y.-K. Kwon, and D. Tománek, Phys. Rev. Lett. **88**, 185502 (2002).